

# Vacancy ordering and phonon spectrum in the Fe superconductor $K_{0.8}Fe_{1.6}Se_2$

A. M. Zhang, K. Liu, J. H. Xiao, J. B. He, D. M. Wang, G. F. Chen, B. Normand, and Q. M. Zhang\*

*Department of Physics, Renmin University of China, Beijing 100872, P. R. China*

(Dated: April 25, 2012)

We have performed Raman-scattering measurements on a high-quality single crystal of the recently discovered Fe-based superconductor  $K_{0.8}Fe_{1.6}Se_2$  ( $T_c = 32$  K). At least thirteen phonon modes were observed in the wave number range  $10$ – $300$   $\text{cm}^{-1}$ . The spectra possess a four-fold symmetry indicative of bulk vacancy order in the Fe-deficient planes. We perform a vibration analysis based on first-principles calculations, which both confirms the ordered structure and allows a complete mode assignment. We observe an anomaly at  $T_c$  in the  $180$   $\text{cm}^{-1}$   $A_g$  mode, which indicates a rather specific type of electron-phonon coupling.

PACS numbers: 74.70.-b, 74.25.Kc, 63.20.kd, 78.30.-j

## I. INTRODUCTION

Since the discovery of high- $T_c$  Fe-based superconductors almost three years ago, much effort has been devoted both to exploring their physical properties and to the search for new materials in this class. Until recently, five such systems had been synthesized and studied, among which  $\text{Fe}(\text{Se},\text{Te})$  is of particular interest as the first Fe-based superconductor not requiring the poisonous element As. Although the superconducting transition temperature ( $T_c$ ) is low, it has been found for  $\text{FeSe}$  that a maximum  $T_c$  of 37 K is obtained under a pressure of 6 GPa.<sup>1</sup> This strong dependence has inspired efforts to find new  $\text{FeSe}$ -based superconductors by introducing internal chemical pressure.<sup>2</sup> This idea was realized very recently in  $K_{0.8}\text{Fe}_2\text{Se}_2$ ,<sup>3</sup> where  $T_c \sim 31$  K is close to that of the “122” materials. The system was also identified as being isostructural with  $\text{BaFe}_2\text{As}_2$ .<sup>3</sup> Several groups have now reported similar  $T_c$  values by substitution of other alkali metals, including Rb and Cs.<sup>4</sup>

The electronic and magnetic properties of the  $A_x\text{Fe}_{2-y}\text{Se}_2$  compounds have been probed extensively. Angle-resolved photoemission spectroscopy (ARPES) measurements<sup>6,7</sup> agree on the presence of one Fermi surface around the M point, and on a conventional  $s$ -wave pairing symmetry, but differ on further details. Nuclear magnetic resonance (NMR) measurements in superconducting crystals find very narrow line widths,<sup>8</sup> strong coupling, singlet superconductivity but with no coherence peak, and very weak spin fluctuations.<sup>8–10</sup> Infrared optical conductivity measurements have identified the parent compound as a small-gap semiconductor and not a Mott insulator.<sup>11</sup> Neutron diffraction studies find a very large ordered moment and high magnetic transition temperature.<sup>12</sup> High-pressure experiments by several groups have led to contradictions which indicate extreme sensitivity to the nature of the defects.<sup>13</sup>

These high-pressure measurements are not the only indications for a crucial role of Fe vacancies. Superconductivity itself occurs only in Fe-deficient samples. A broad resistivity peak around 150 K is reduced dramatically by altering the Fe content.<sup>5</sup> The unexpected abundance of infrared-active phonon modes<sup>11</sup> may also be attributed

to Fe vacancies. Resolving the distribution of Fe vacancies on the microscopic level is clearly essential for a full understanding of the electronic and magnetic properties. A study exploiting the unique sensitivity of Raman scattering to probe local lattice symmetries is thus required.

Here we measure Raman-scattering spectra in a high-quality superconducting crystal of  $K_{0.8}Fe_{1.6}Se_2$ , as described in Sec. II. Our results, presented in Sec. III, contain at least thirteen phonon modes, far more than would be expected for a normal 122 structure. The spectra we obtain by rotating the crystal show a four-fold symmetry, which we identify as  $C_{4h}$  or  $C_4$ . These results indicate an ordered structure of Fe vacancies, and in Sec. IV we assume the highest-symmetry defect configuration to perform a first-principles vibration analysis. The calculated mode frequencies and symmetry assignments are fully consistent with our data, confirming completely the vacancy ordering pattern. Our temperature-dependent spectra, shown in Sec. V, reveal one specific  $A_g$  mode with a clear frequency jump at  $T_c$ , which suggests a close connection between phonons and superconductivity. Section VI contains a brief summary.

## II. MATERIAL AND METHOD

The crystal was grown by the Bridgeman method. The detailed growth procedure may be found elsewhere.<sup>5</sup> The most accurate available composition determination is the neutron diffraction refinement,<sup>12</sup> which gives  $K_{0.8}Fe_{1.6}Se_2$ . X-ray diffraction patterns indicate no discernible secondary phase. The resistivity was measured by a Quantum Design PPMS and the magnetization by the PPMS vibrating sample magnetometer (VSM): both quantities, shown in the inset of Fig. 1, exhibit transitions at  $T_c \sim 32$  K, the diamagnetic transition appearing particularly sharp. Although the precise demagnetization factor is not available, the estimated superconducting volume fraction is (from the sharp diamagnetism and absence of a secondary phase) close to 100%. These results indicate that the crystal is of very high quality.

The crystal was cleaved in a glove box and a flat, shiny surface was obtained. The surface is parallel to

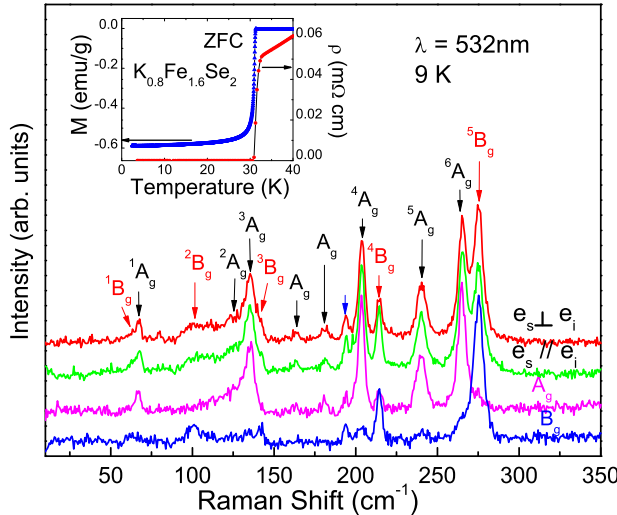


FIG. 1: (Color online) Raman spectra of a  $K_{0.8}Fe_{1.6}Se_2$  crystal at 9 K. Labels  $e_i$  and  $e_s$  denote the incident and scattered light polarizations. Black and red arrows indicate respectively the assigned  $A_g$  and  $B_g$  modes, the blue arrow a weak mode whose symmetry remains unknown. The accumulation time for the cross-polarization measurements is approximately three times that in parallel polarization. The spectra labeled  $A_g$  and  $B_g$  were measured by controlling the relative angle between the incident and scattered light polarizations once the mode symmetries had been assigned; this assignment was performed by combining rotation measurements (Fig. 2) with the formal symmetry analysis [Eq. (1)]. Inset: resistivity and magnetization data for the same crystal.

the  $(ab)$ -plane, and forms the basal plane for our Raman measurements. The two pieces of freshly-cleaved crystal were sealed under an argon atmosphere: one was transferred into the cryostat within 30 seconds for Raman-scattering studies and the other used for symmetry investigations by rotating the crystal. The cryostat was evacuated immediately to a work vacuum of approximately  $10^{-8}$  mbar. Raman measurements were performed in a pseudo-backscattering configuration with a triple-grating monochromator (Jobin Yvon T64000), delivering a spectral resolution better than  $0.6\text{ cm}^{-1}$ . The light source is a 532 nm solid-state laser (Torus 532, Laser Quantum) whose beam was focused into a spot of diameter  $ca.$   $10\text{--}20\text{ }\mu\text{m}$  on the sample surface. The beam power is lower than 1 mW, and the real temperature at the spot was calibrated using the intensity relation between the Stokes and anti-Stokes spectra.

### III. PHONON RAMAN SPECTRA: SYMMETRY AND VACANCY ORDER

The phonon modes of  $K_{0.8}Fe_{1.6}Se_2$  are shown in the low-temperature spectra of Fig. 1. The most striking feature is that at least thirteen modes are present in the spectra collected with both parallel and cross-

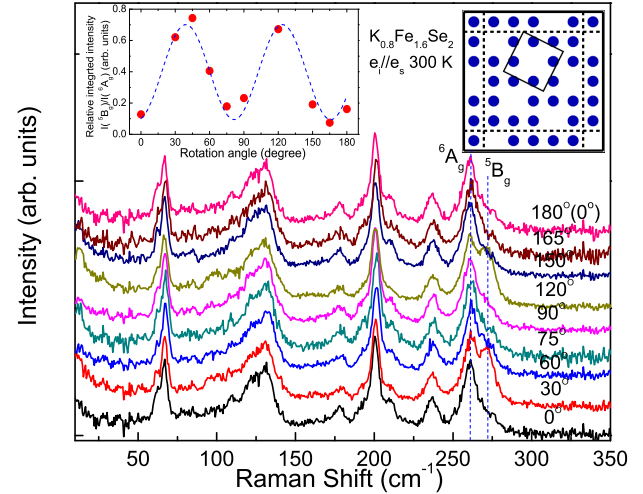


FIG. 2: (Color online) Raman spectra obtained by rotation, collected in air at room temperature immediately after cleavage. The zero-degree point is chosen arbitrarily (not measured relative to the crystal principal axes). Dashed lines mark two modes, labeled as  $^5B_g$  and  $^6A_g$ , whose relative integrated intensity variation is shown as a function of angle in the left inset [the dashed line has the form  $\sin^2 2\theta$ ]. Right inset: schematic representation of ordered vacancy configuration with 20% Fe deficiency and four-fold symmetry.

polarization configurations. All of these modes are located below  $300\text{ cm}^{-1}$  (Fig. 4 illustrates this most clearly). Our results are therefore consistent both by number and location with the infrared optical spectra.<sup>11</sup> We stress that only four Raman-active modes are present in 122,<sup>14</sup> to which  $K_{0.8}Fe_{1.6}Se_2$  was thought to be isostructural, and that the spectra of Fig. 1 are completely different from those observed in  $Fe(Se,Te)$ .<sup>15</sup> The surprisingly large number of Raman and infrared phonon modes reinforces the assumption that the Fe deficiency drives a local breaking of lattice symmetry. A vibration analysis of the modes in Fig. 1, which we perform below, is thus significantly more complicated than for 122 and requires additional structural information.

In Fig. 2 we present spectra obtained by rotating the crystal. These display clearly a four-fold symmetry, which is highlighted in the right inset. A formal analysis based on four-fold symmetry proceeds as follows. There are two possible Raman tensors, one for  $C_{4h}/C_4$  and the other for  $D_{4h}/D_4$ .<sup>25</sup> If  $\theta$  is defined as the angle between the crystallographic  $a$ -axis and the polarization of the incident light, and  $\varphi$  as the angle between the polarizations of the incident and scattered light, then the angle-dependences of the Raman intensities for  $C_{4h}/C_4$  take the form

$$\begin{aligned} I_{A_g} &= |a \cos(\varphi) + c \sin(\varphi)|^2, \\ I_{B_g} &= |d \cos(\varphi + 2\theta) + e \sin(\varphi + 2\theta)|^2, \end{aligned} \quad (1)$$

where  $a$ ,  $c$ ,  $d$ , and  $e$  are matrix elements of the Raman tensors, and depend on linear combinations of polariz-

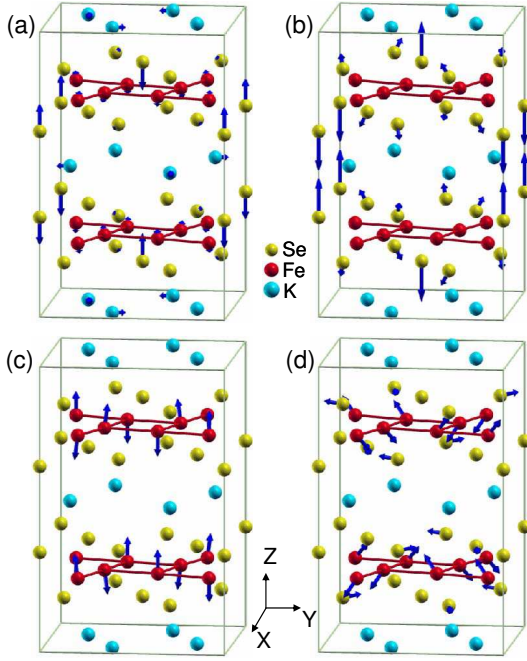


FIG. 3: (Color online) Displacement patterns for selected Raman-active  $A_g$  [(a) and (b), labeled as  $^1A_g$  and  $^4A_g$  in Table I] and  $B_g$  modes [(c) and (d), labeled as  $^4B_g$  and  $^5B_g$  in Table I] of  $K_{0.8}Fe_{1.6}Se_2$ . Fe atoms connected by red lines have right-handed chirality. Amplitude arrows in (d) are scaled up by a factor of 1.4 over the other panels. Atomic structures and displacement patterns prepared using XCRYSDEN.<sup>24</sup>

ability derivatives for the atoms involved in each mode. Similarly, for  $D_{4h}/D_4$  one has

$$I_{A_{1g}} = |a \cos(\varphi)|^2, \quad I_{B_{1g}} = |e \sin(\varphi + 2\theta)|^2. \quad (2)$$

Because rotating the crystal varies the angle  $\theta$ , it is clear that modes with constant intensities are all  $A$ -type ( $A_{1g}$ ,  $A_g$ ,  $A_1$ , or  $A$ ), while those showing an intensity modulation are  $B$ -type. Further, Eq. (2) prohibits the observation of  $A$ -type modes in  $D_{4h}$  symmetry in a cross-polarized configuration ( $\varphi = \pi/2$ ), which contradicts the observations in Fig. 1. Thus our results exclude explicitly the  $D_{4h}$  symmetry expected for the 122 structure, and allow us to deduce that the crystal symmetry is  $C_{4h}$  or  $C_4$ . The  $A$ -type modes in Fig. 1 may therefore be identified as  $A_g$  or  $A$  phonons. This symmetry constrains very strongly the possible vacancy ordering patterns.

Indications for vacancy ordering in  $A_xFe_{2-y}Se_2$  systems have been obtained in several recent measurements. Imaging by transmission electron microscopy (TEM)<sup>17</sup> reveals rather well-defined surface order for  $y = 0.5$  and  $y = 0.2$ . NMR measurements<sup>10</sup> find additional line-splittings. While Raman scattering is a surface technique, the wavelength, laser spot size (10-20  $\mu\text{m}$ ), and penetration depth mean that macroscopic symmetries are probed. The 20% vacancy concentration in our crystal ( $y = 0.4$ ) suggests the structure illustrated in the inset of Fig. 2: this arrangement has a  $\sqrt{5} \times \sqrt{5}$  unit cell, has

local four-fold symmetry, and, crucially, has lost the two mirror planes perpendicular to the  $(ab)$ -plane, in complete consistency with our Raman measurements. This microscopic structure has been demonstrated spectacularly by the very recent neutron diffraction studies of Ref. 12. X-ray diffraction studies of several crystals with  $y = 0.37$ – $0.39$  have confirmed this result.<sup>18</sup>

#### IV. FIRST-PRINCIPLES CALCULATIONS

To compare with the observed phonon modes, we have calculated the nonmagnetic electronic structure and zone-center phonons of  $K_{0.8}Fe_{1.6}Se_2$  from first-principles density functional calculations. We use the Vienna *ab initio* simulation package,<sup>20</sup> which is based on the projector augmented wave (PAW) method<sup>21</sup> with a general gradient approximation (GGA)<sup>22</sup> for exchange-correlation potentials. The structural information determined by neutron diffraction<sup>12</sup> is that  $K_{0.8}Fe_{1.6}Se_2$  has space group  $I4/m$  and point group  $C_{4h}$ . The Wyckoff positions of the K, Fe, and Se atoms and the corresponding symmetry analysis are listed in Table I. The frequencies and displacement patterns of the phonon modes were calculated using the dynamical matrix method.<sup>23</sup>

In total, 17  $A_g$  and  $B_g$  modes are allowed by the crystal symmetry, among which 11 of the modes in the polarized Raman spectra of Fig. 1 may be assigned accurately from the calculations (Table I). The vibration patterns of selected modes are shown in Fig. 3. The cal-

TABLE I: Symmetry analysis for  $I4/m$  and assignment of Raman-active vibration modes in  $K_{0.8}Fe_{1.6}Se_2$

Atom	Wyckoff position	Optical modes		
		Raman active	Infrared active	
K	8h	$2A_g + 2B_g + 2E_g$	$A_u + 4E_u$	
Fe	16i	$3A_g + 3B_g + 6E_g$	$3A_u + 6E_u$	
Se	4e	$A_g + 2E_g$	$A_u + 2E_u$	
Se	16i	$3A_g + 3B_g + 6E_g$	$3A_u + 6E_u$	
Expt. Freq. (cm <sup>-1</sup> )	Cal. Freq. (cm <sup>-1</sup> )	Symmetry	Atoms	Index
61.4	66.7	$B_g$	Se	$^1B_g$
66.3	75.1	$A_g$	Se	$^1A_g$
100.6	106.2	$B_g$	K	$^2B_g$
123.8	130.5	$A_g$	Se	$^2A_g$
134.6	159.2	$A_g$	Se	$^3A_g$
141.7	149.0	$B_g$	Se	$^3B_g$
202.9	212.6	$A_g$	Se	$^4A_g$
214.3	238.3	$B_g$	Fe	$^4B_g$
239.4	268.5	$A_g$	Fe	$^5A_g$
264.6	286.1	$A_g$	Fe,Se	$^6A_g$
274.9	279.0	$B_g$	Fe	$^5B_g$

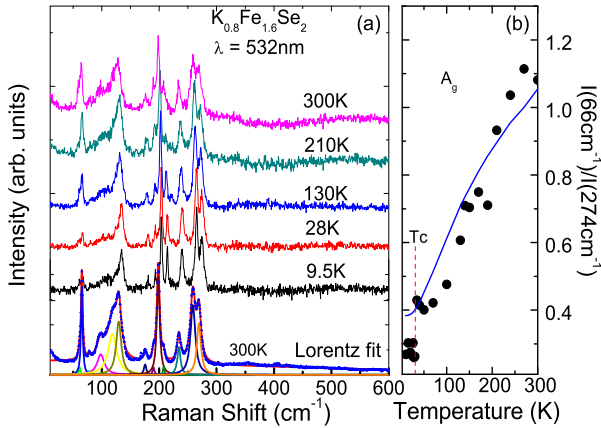


FIG. 4: (Color online) (a) Raman spectra at selected temperatures. An example of fitting with Lorentz functions is shown at the base of the panel for 300 K data collected in parallel polarization with an accumulation time four times that of the other spectra. The frequency resolution is then  $0.3 \text{ cm}^{-1}$ , which allows the explicit separation of 13 modes in the narrow frequency interval  $50$ – $300 \text{ cm}^{-1}$ . The fits used to obtain the data points in Figs. 4(b) and 5 have a coefficient of determination  $r^2 > 0.95$ . (b) Temperature-dependence of the relative intensities of the  $66 \text{ cm}^{-1}$  and  $274 \text{ cm}^{-1}$  modes. The solid line shows the Bose-Einstein thermal factor.

culated phonon frequencies,  $75.1$  and  $212.6 \text{ cm}^{-1}$  for  $A_g$  modes [Fig. 3(a) and (b)] and  $238.3$  and  $279.0 \text{ cm}^{-1}$  for  $B_g$  modes [Fig. 3(c) and (d)], agree very well with the  $66.3$ ,  $202.9$ ,  $214.3$ , and  $274.9 \text{ cm}^{-1}$  modes in the experimental measurements. The  $A_g$  and  $B_g$  modes shown in Figs. 3(b) and (c) correspond exactly to the  $A_{1g}$  mode of As and  $B_{1g}$  mode of Fe in the 122 system.<sup>14</sup> The success of the phonon assignment confirms completely the assumed pattern of vacancy ordering. Only three of the observed 13 modes cannot be assigned well, even though two have  $A_g$  character. We suggest that these may originate from distortions of the Fe-Se layer, which lie outside the symmetry constraints applied.

## V. TEMPERATURE-DEPENDENT SPECTRA

We have also measured Raman spectra over the full temperature range to 300 K [Fig. 4(a)]. The temperature-dependence of the phonon modes is described explicitly by fitting with Lorentz functions. All relative intensities show a conventional phonon form, with one exception (below). This line-shape analysis shows no evidence of the Fano asymmetry characteristic of electron-phonon coupling. However, all of the phonons are rather broad when compared with those in 122 systems,<sup>14</sup> due perhaps to intrinsic disorder (incompletely ordered vacancies). This analysis alone cannot therefore exclude a generic electron-phonon coupling in  $K_{0.8}Fe_{1.6}Se_2$ .

The  $A_g$  mode at  $66 \text{ cm}^{-1}$  behaves rather anomalously.

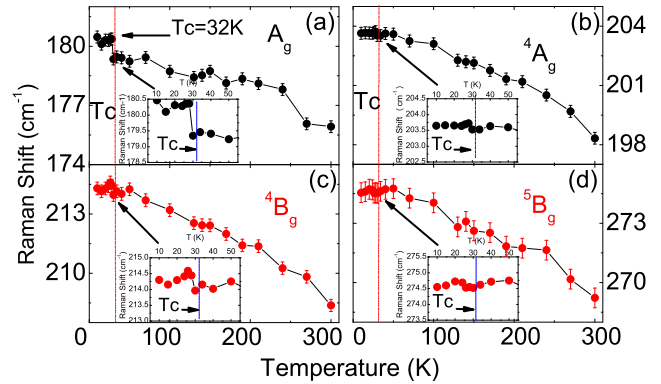


FIG. 5: (Color online) (a)-(d) Temperature-dependence of phonon frequencies for four modes with the highest measured intensities. Insets magnify the region around  $T_c$ . Horizontal and vertical scales are the same in all panels and insets.

The steep fall in its relative intensity [Fig. 4(b)] follows a Bose-Einstein form only to lowest order, but with significant deviations. In addition to a clear intensity jump at  $T_c$ , there is a further apparent anomaly around 160 K, where X-ray diffraction studies find no structural transition.<sup>13</sup> We have confirmed (Table I) that the  $66 \text{ cm}^{-1}$  phonon is the vibration mode of a Se atom, and suggest that this is the origin of its unusual behavior.

The temperature-dependence of selected phonon frequencies is shown in Fig. 5. The superconducting transition has very little effect on the frequency in every case but one: the  $A_g$  mode at  $180 \text{ cm}^{-1}$  exhibits a clear jump of approximately  $1 \text{ cm}^{-1}$  at  $T_c$  [Fig. 5(a)]. This anomaly is definite evidence for a particular type of connection between phonons and superconductivity, and it constitutes a statement concerning both symmetry and energies. For the former, the symmetry relation between the superconducting gaps on the available Fermi surfaces should be consistent with  $A_g$ . For the latter, we suggest that a coupling of this phonon mode to the superconducting quasiparticles may be visible<sup>19</sup> in ARPES spectra, where it should be expected at energies  $E \sim 20$ – $25 \text{ meV}$  and at the  $\Gamma$  point (the part of the Brillouin zone probed by Raman scattering). Anomalous features are indeed present in this region in the two most recent ARPES studies of  $A_xFe_{2-y}Se_2$  superconductors,<sup>7</sup> and we propose that high-resolution ARPES measurements may reveal the physics behind this phenomenon.

## VI. SUMMARY

To conclude, we have performed Raman-scattering measurements on the recently discovered Fe-based superconductor  $K_{0.8}Fe_{1.6}Se_2$ . Using a high-quality single crystal, we find that there exist at least thirteen phonon modes and that the spectra have four-fold symmetry. This demonstrates the presence of long-range-ordered configurations of Fe vacancies, which dictate the local lat-

tice vibrations. We perform first-principles calculations to obtain a complete and consistent phonon assignment, confirming the nature of the vacancy ordering pattern. We find that only one mode exhibits a change in frequency around  $T_c$ , suggesting a rather specific connection between superconductivity and lattice vibrations.

### Acknowledgments

We thank W. Bao and Z. Y. Lu for helpful discussions. This work was supported by the 973 program

under Grant No. 2011CBA00112, by the NSF of China under Grant Nos. 11034012 and 11004243, by the Fundamental Research Funds for Central Universities, and by the Research Funds of Renmin University.

---

\* Electronic address: qmzhang@ruc.edu.cn

<sup>1</sup> S. Margadonna *et al.*, Phys. Rev. **80**, 064506 (2009).

<sup>2</sup> M. K. Wu *et al.*, Physica C **469**, 340 (2009).

<sup>3</sup> J. G. Guo *et al.*, Phys. Rev. B **82**, 180520(R) (2010).

<sup>4</sup> Y. Mizuguchi *et al.*, Appl. Phys. Lett. **98**, 042511 (2011); A. Krzton-Maziopa *et al.*, J. Phys.: Condens. Matter **23**, 052203 (2011); A. F. Wang *et al.*, Phys. Rev. B **83**, 060512(2011); J. J. Ying *et al.*, Phys. Rev. B **83**, 212502(2011); C. H. Li *et al.*, Phys. Rev. B **83**, 184521(2011); H. D. Wang *et al.*, Europhys. Lett. **93**, 47004 (2011).

<sup>5</sup> D. M. Wang, J. B. He, T.-L. Xia, and G. F. Chen, Phys. Rev. B **83**, 132502(2011).

<sup>6</sup> Y. Zhang *et al.*, Nature Materials **10**, 273 (2011); T. Qian *et al.*, Phys. Rev. Lett. **106**, 187001(2011).

<sup>7</sup> D. X. Mou *et al.*, Phys. Rev. Lett. **106**, 107001(2011); X. P. Wang *et al.*, Europhys. Lett. **93**, 57001 (2011).

<sup>8</sup> W. Yu *et al.*, Phys. Rev. Lett. **106**, 197001(2011).

<sup>9</sup> H. Kotegawa *et al.*, J. Phys. Soc. Jpn. **80**, 043708(2011).

<sup>10</sup> D. A. Torchetti *et al.*, Phys. Rev. B **83**, 104508(2011).

<sup>11</sup> Z. G. Chen *et al.*, Phys. Rev B **83**, 220507(R) (2011).

<sup>12</sup> W. Bao *et al.*, Chin. Phys. Lett. **28**, 086104 (2011).

<sup>13</sup> J. Guo *et al.*, unpublished (arXiv:1101.0092); Y. Kawasaki *et al.*, unpublished (arXiv:1101.0896); J. J. Ying *et al.*, New J. of Phys. **13**, 033008(2011).

<sup>14</sup> A. P. Litvinchuk *et al.*, Phys. Rev. B **78**, 060503 (2008).

<sup>15</sup> T.-L. Xia *et al.*, Phys. Rev. B **79**, 140510(R) (2009).

<sup>16</sup> O. Tiedje *et al.*, Phys. Rev. B **67**, 134105 (2003).

<sup>17</sup> Z. Wang *et al.*, Phys. Rev. B **83**, 140505(R) (2011).

<sup>18</sup> P. Zavalij *et al.*, Phys. Rev. B **83**, 132509 (2011).

<sup>19</sup> Z. X. Shen, A. Lanzara, S. Ishihara, and N. Nagaosa. Phil. Mag. B **82**, 1349 (2002).

<sup>20</sup> G. Kresse and J. Hafner, Phys. Rev. B **47**, 558 (1993); G. Kresse and J. Furthmüller, *ibid.* **54**, 11169 (1996).

<sup>21</sup> P. E. Blöchl, Phys. Rev. B **50**, 17 953 (1994); G. Kresse and D. Joubert, Phys. Rev. B **59**, 1758 (1999).

<sup>22</sup> J. P. Perdew, K. Burke, and M. Ernzerhof. Phys. Rev. Lett. **77** 3865 (1996).

<sup>23</sup> K. Liu and S. Gao, Phys. Rev. Lett. **95**, 226102 (2005).

<sup>24</sup> A. Kokalj, Comp. Mater. Sci. **28**, 155 (2003).

<sup>25</sup> W. Hayes and R. Loudon, *Scattering of Light by Crystals* (John Wiley, New York, 1978).